Research Square

Preprints are preliminary reports that have not undergone peer review.
They should not be considered conclusive, used to inform clinical practice,
or referenced by the media as validated information.

Time-Resolved Multi-Omic Characterization of Post-Thaw Remodeling in Monocytic THP-1 Cells

Lukas Underwood
American Type Culture Collection
Ajeet P. Singh
American Type Culture Collection
Noah Wax
American Type Culture Collection
Stephen King
American Type Culture Collection
Jacqueline Mikhaylov
American Type Culture Collection
Jonathan L. Jacobs
American Type Culture Collection
Nilay Chakraborty
nchakraborty@atcc.org

American Type Culture Collection

Article

Keywords:

Posted Date: November 11th, 2026

DOI: https://doi.org/10.21203/rs.3.rs-11377893/v1

License: This work is licensed under a Creative Commons Attribution 4.0 International License.
Read Full License

Additional Declarations: Competing interest reported. All authors are employees of ATCC. ATCC develops and distributes the THP-1 cell products evaluated in this study. The authors declare no other competing interests.

Time-Resolved Multi-Omic Characterization of Post-Thaw Remodeling in Monocytic THP-1 Cells

Lukas Underwood†, Ajeet P. Singh†, Noah Wax, Stephen King, Jacqueline Mikhaylov, Jonathan L. Jacobs*, Nilay Chakraborty*

ATCC, 10801 University Boulevard, Manassas, Virginia 20110-2209, USA

† These authors contributed equally.

*Correspondence:
Jonathan L. Jacobs: jjacobs@atcc.org
Nilay Chakraborty: nchakraborty@atcc.org

Abstract

Cryopreserved cells are increasingly used as standardized experimental inputs, yet cells used shortly after thaw may remain in a dynamically changing biological state. We used THP-1 cells to define this post-thaw state and determine how it relates to assay-ready function. Time-resolved transcriptomic profiling compared independently produced standard-vial and assay-ready preparations during the first 8 h after thaw, while complementary proteomic profiling followed shared-harvest preparations through 72 h. Functional behavior was evaluated using an assay-ready NF-κB reporter model.

Post-thaw progression was characterized by organized, time-dependent molecular remodeling. Transcriptional responses were rapid and broad, whereas proteomic changes developed more gradually. Standard and assay-ready preparations predominantly engaged shared inflammatory, stress, proliferative, and metabolic programs, while differing in the magnitude and persistence of selected responses. Differences present immediately after thaw in independently produced materials, together with minimal direct divergence in the shared-harvest proteomic experiment, support a contribution of upstream cellular state to post-thaw phenotype. Despite ongoing molecular remodeling, assay-ready cells retained robust lipopolysaccharide-induced NF-κB responsiveness, although response magnitude depended on post-plating timing.

These findings identify the post-thaw period as a structured biological transition and show that assay readiness can coexist with molecular nonequivalence when functional performance is maintained within a defined use window.

Introduction

Cryopreserved cell lines are widely used as standardized experimental inputs in biomedical research, biotechnology, and drug discovery. Banking defined cell populations can reduce the variability associated with continuous culture and provide

reproducible starting materials across experiments and over time[1,2]. Assay-ready formats extend this concept by enabling cells to enter an experiment shortly after thaw, with little or no intervening expansion. However, cryopreservation is not biologically neutral. Cryoprotectant exposure, freezing, thawing, and subsequent adaptation can perturb oxidative balance, membrane and cytoskeletal organization, survival signaling, metabolism, and gene expression[3–6]. These effects may be transient, and their magnitude and persistence can vary with cell type, freezing protocol, starting cell state, and recovery conditions[6]. For cells used within hours of thaw, however, the transient state itself becomes part of the experimental input. The relevant question is therefore not only whether cells survive cryopreservation, but how their biological state evolves after thaw and whether ongoing remodeling alters the functional phenotype measured during the intended use window.

THP-1 cells provide a useful model for addressing this problem. This human monocytic leukemia-derived cell line is widely used to investigate monocyte and macrophage biology, innate immune signaling, inflammation, and pharmacologic responses[7–9]. Many of these applications depend on rapidly inducible pathways whose output is sensitive to the physiological state of the cells at the time of stimulation. THP-1 cells therefore provide an opportunity to examine post-thaw remodeling across molecular layers while also testing whether substantial molecular change is compatible with assay-relevant immune function.

An important consideration is that cell-line identity does not necessarily imply biological-state equivalence at the point of experimental use. Preparations derived from the same cell line can differ in expansion history, culture state, formulation, and preservation workflow, potentially capturing distinct cellular states at the time of freezing. Cryopreservation may preserve aspects of this upstream biological history rather than reset the cells to a common state. Conversely, differences observed after thaw may also arise from the preservation process itself or from subsequent adaptation to the post-thaw environment. Distinguishing these contributions is particularly important for assay-ready systems, in which the thawed population itself serves as the experimental input rather than an intermediate that is returned to prolonged culture.

Despite the widespread use of cryopreserved cell systems, the immediate post-thaw interval remains incompletely resolved at the molecular level. Post-thaw behavior is often evaluated using viability, recovery, or endpoint functional measurements, yet these metrics provide limited information about how the underlying cellular state changes over time. Transcriptomic measurements can capture rapid regulatory responses, whereas protein-abundance measurements reflect slower processes involving translation, degradation, and persistence of pre-existing protein pools. Functional measurements provide a further level of resolution by determining whether molecular nonequivalence

translates into altered biological performance. Integrating these layers therefore offers a framework for distinguishing a coordinated post-thaw state transition from isolated measures of cryoinjury or recovery.

Here, we used complementary time-resolved transcriptomic, proteomic, and functional analyses to define post-thaw remodeling in THP-1 cells. Transcriptomic profiling compared independently produced standard-vial and assay-ready preparations during acute recovery, while proteomic profiling followed shared-harvest preparations through preservation and 72 h post-thaw. Finally, an assay-ready NF-κB luciferase reporter model was used to evaluate inducible inflammatory signaling under defined post-thaw conditions. Rather than treating cryopreservation as a single before-versus-after perturbation, these complementary designs allowed us to ask whether cryopreserved cells traverse a structured post-thaw biological transition, which components of that response are broadly conserved or context dependent, and whether ongoing molecular remodeling is compatible with assay-ready functional responsiveness.

Results

Complementary designs resolve distinct components of the post-thaw state

To examine how cellular state changes following cryopreservation, we used complementary transcriptomic and proteomic designs that resolved different components of the post-thaw response (Fig. 1).

For transcriptomic analysis, STD and AR THP-1 preparations generated from independently prepared starting pools were sampled at 0, 2, and 8 h post-thaw. Because the two preparations differed in both upstream culture history and preservation workflow, these comparisons captured the biological states delivered by each format as they would be encountered experimentally. An additional STD-derived culture maintained for 6 days after thaw served as a later recovered reference.

For proteomic analysis, a common THP-1 harvest was divided between STD and AR preservation conditions, reducing differences in pre-freeze cellular state. Samples were collected at harvest, after a 2-h cryoprotectant-medium hold, immediately after thaw, and at 24 and 72 h post-thaw. A non-frozen continued-culture arm was collected 72 h after harvest (CC-72 h). This design more directly resolved changes associated with processing, freeze-thaw, and subsequent post-thaw progression.

Together, the two workflows provided complementary views of the post-thaw state: the transcriptomic analysis captured differences present in independently produced cell inputs during the acute post-thaw interval, whereas the shared-harvest proteomic analysis constrained differences arising before preservation and followed molecular remodeling over a longer period.

Post-thaw progression organizes molecular state across transcriptomic and proteomic layers

Principal component analysis revealed strong temporal organization in both molecular datasets (Fig. 2). In the transcriptomic analysis, STD and AR samples followed a clear post-thaw trajectory rather than separating primarily by preservation format (Fig. 2a). At 0 h, both formats occupied a region near the 6-day recovered reference. By 2 h, STD and AR samples shifted markedly along PC1, and by 8 h they moved predominantly along PC2 rather than returning directly toward the 0-h or recovered-reference state. Although STD and AR remained distinguishable within individual time points, post-thaw time was the dominant global feature of the transcriptomic structure.

Proteomic changes were more gradual but similarly time organized (Fig. 2b). Harvest, AR hold, STD hold, and AR-0 h samples occupied a compact early-state region, whereas STD-0 h was shifted toward the later post-thaw samples. The 24- and 72-h groups occupied distinct regions of the PCA space, and CC-72 h shared some movement with the 72-h post-thaw samples while remaining separated from them. Thus, continued culture and post-thaw progression generated related but nonidentical later proteomic states.

Variance partitioning was consistent with these global patterns (Fig. 2c). Using an order-independent decomposition of feature-level variance, time accounted for the largest median component of transcriptomic variation (0.753), followed by condition (0.079), interaction (0.033), and residual variation (0.052). Time was also the largest modeled component for 85.7% of retained genes. In the proteomic dataset, time remained the largest median component (0.486), whereas condition contributed comparatively little (0.013); interaction and residual components were larger than in the transcriptomic dataset. Time was the largest modeled component for 86.1% of proteins. These analyses identify elapsed time as the primary organizing factor of molecular state following thaw, with a more sharply resolved temporal structure at the transcript level.

Post-thaw responses are directionally conserved across preservation contexts

We next asked whether STD and AR cells engaged similar molecular responses despite differences in their starting states (Fig. 3). Relative to the 6-day recovered reference, substantial numbers of differentially expressed genes (DEGs) were detected in both formats throughout the acute post-thaw interval (Fig. 3a). At 0 h, 1,656 DEGs were detected in STD cells and 842 in AR cells. DEG burden increased sharply at 2 h to 3,278 and 3,019 genes, respectively, before declining at 8 h to 2,498 in STD and 2,604 in AR.

Despite differences in DEG number, the direction of transcriptional change was strongly conserved. Among genes meeting the DEG criteria in at least one format, 93.9%

changed in the same direction at 0 h (R^2 = 0.578; Fig. 3b). Directional concordance increased to 97.3% at 2 h, together with substantially stronger agreement in fold-change magnitude (R^2 = 0.886; Fig. 3c) and remained high at 8 h (Supplementary Fig. S1).

Proteomic responses were smaller in feature number but showed a similar increase followed by decline in differential-abundance burden (Fig. 3d). Relative to CC-72 h, 17 differentially abundant proteins (DAPs) were detected in STD cells and 8 in AR cells immediately after thaw. DAP numbers increased to 57 and 55, respectively, at 24 h before declining to 18 and 22 at 72 h.

Proteomic concordance was weakest immediately after thaw, when 72.2% of proteins changed in the same direction and agreement in magnitude was low (R^2 = 0.156; Fig. 3e). By 24 h, directional concordance reached 100% with substantially stronger agreement in fold-change magnitude (R^2 = 0.848; Fig. 3f), and high concordance persisted at 72 h (96.2%; Supplementary Fig. S1).

Thus, STD and AR cells predominantly engaged shared post-thaw trajectories, with preservation context influencing response magnitude, particularly at early time points.

Shared trajectories coexist with context-dependent transcriptional states

Strong directional concordance did not imply that STD and AR cells occupied equivalent molecular states. Direct comparison at matched time points identified 505 DEGs between STD and AR cells at 0 h, 551 at 2 h, and 744 at 8 h (Fig. 4a). Gene-level overlap showed both persistence and turnover, with 103 genes differentially expressed at all three time points and additional time-specific components (Fig. 4b).

At the pathway level, differences between the independently produced formats were considerably more persistent (Fig. 4c). Proliferative programs including E2F targets, MYC targets, and G2M checkpoint remained enriched in STD cells, whereas inflammatory and stress-associated programs including TNFα signaling via NF-κB, inflammatory response, interferon responses, and apoptosis remained relatively enriched in AR cells. Eighteen Hallmark pathways were significantly different between formats at all three time points, and 27 of the 33 pathways significant at any time point were shared by at least two comparisons (Fig. 4d).

In contrast, direct proteomic differences between STD and AR cells were minimal when both conditions originated from the same harvest (Fig. 4e). No DAPs were identified after the pre-freeze hold, six were detected immediately after thaw, none at 24 h, and one at 72 h.

These results show that independently produced STD and AR preparations can retain distinct transcriptional states while undergoing strongly aligned post-thaw responses. The limited direct proteomic divergence under a shared-harvest design is consistent

with a contribution of upstream cellular context to the molecular differences observed between independently produced frozen inputs.

Post-thaw remodeling proceeds through phased biological programs across molecular layers

Hallmark enrichment analysis revealed that the post-thaw response was organized into biological programs with distinct temporal behavior (Fig. 5). During the first 2 h, inflammatory and stress-associated pathways were broadly positively enriched, followed by reversal or attenuation between 2 and 8 h (Fig. 5a). TNFα signaling via NF-κB exemplified this pattern, with a mean normalized enrichment score (NES) across STD and AR cells of 2.12 from 0 to 2 h and −2.36 from 2 to 8 h.

Proliferation-associated pathways showed the opposite temporal pattern. E2F targets were strongly negatively enriched during the first 2 h (mean NES = −2.32) and shifted positively between 2 and 8 h (mean NES = 1.90). G2M checkpoint showed a similar early-negative to later-positive transition, whereas other programs, including interferon-γ response and protein secretion, remained positively enriched across both intervals. Comparison of the early and later intervals therefore separated transient responses from programs that remained directionally sustained (Fig. 5c).

Proteomic enrichment was narrower but retained clear temporal structure (Fig. 5b,d). E2F targets again exhibited an early-negative to later-positive transition, with a mean NES of −1.65 from 0 to 24 h and 1.58 from 24 to 72 h. Complement, coagulation, and IL-2–STAT5 signaling showed the inverse pattern, whereas cholesterol homeostasis remained negatively enriched across the proteomic interval.

Among the seven Hallmark pathways represented in both displayed transcriptomic and proteomic summaries, six showed the same enrichment direction at 8 h at the RNA level and 24 h at the protein level (Fig. 5e). These observations support a temporally layered post-thaw response in which broad early transcriptional remodeling is followed by a narrower but biologically organized proteomic response.

Targeted stress responses reveal conserved and context-sensitive components of remodeling

To resolve specific processes within the broader pathway response, we examined a targeted panel of 37 cryostress-associated genes (Fig. 6a). The panel revealed substantial remodeling during the first 8 h, including responses associated with oxidative and metabolic stress, proteostasis, endoplasmic-reticulum stress, membrane regulation, survival, and protein clearance. Several markers also differed between STD and AR cells at 0 h, consistent with the distinct transcriptional states observed before substantial post-thaw progression had occurred.

Representative trajectories illustrated both highly conserved and context-sensitive responses (Fig. 6d). ANXA1 showed closely overlapping induction in STD and AR cells, whereas DDIT4 increased strongly during the early interval in both formats before declining by 8 h. In contrast, HSPA1A and HSPA5 showed greater transcriptional induction in AR cells, while HMOX1 increased in both formats but diverged more strongly by 8 h.

Despite these marker-specific differences, the overall targeted response was highly conserved. Across all 37 markers, STD and AR fold changes were strongly correlated at both 2 h (Pearson r = 0.91, $p = 3.1 \times 10^{-15}$) and 8 h (r = 0.88, $p = 5.5 \times 10^{-13}$; Fig. 6b,c).

Twenty-one markers were also detected in the proteomic dataset (Fig. 6e). Later protein-level changes were more restricted than the early transcriptional response and were generally similar between STD and AR cells. ANXA1 and ANXA2 showed among the largest increases, together with antioxidant-associated proteins including NQO1, GCLM, and SOD2, whereas changes in several proteostasis-associated proteins were comparatively modest.

The targeted analysis therefore resolved a strongly shared core stress response while identifying individual modules whose magnitude or persistence varied with experimental context.

Assay-ready cells retain inducible NF-κB responsiveness while assay timing shapes response magnitude

We next asked whether ongoing post-thaw remodeling was compatible with inducible immune signaling using an NF-κB luciferase reporter THP-1 model (Fig. 7). Assay-ready preparations were compared with non-frozen cultured cells derived from the same reporter line and production pool and processed in parallel at the corresponding harvest state.

LPS concentration strongly influenced NF-κB reporter activity in both formats (Greenhouse–Geisser-corrected repeated-measures ANOVA, F(1.19, 2.39) = 43.96, p = 0.0135; Fig. 7b). Neither the overall format effect (p = 0.518) nor the concentration-by-format interaction (p = 0.0707) was significant, indicating broadly similar concentration-dependent responses.

Stimulation duration also strongly influenced reporter activity (F(1.19, 3.56) = 234.64, p < 0.001; Fig. 7c). Both formats followed a similar overall temporal pattern, with rapid induction, maximal activity near 4 h, and declining responses during prolonged stimulation. A significant format-by-duration interaction was nevertheless detected (F(1.43, 4.28) = 20.12, p = 0.0078), reflecting greater reporter activity in cultured cells at 2 and 3 h (Holm-adjusted p = 0.0113 and p = 0.0404, respectively). Responses were not significantly different between formats at later time points.

Post-plating rest time was also a strong determinant of reporter magnitude ($F(1.33, 3.98) = 44.49$, $p = 0.0023$; Fig. 7d). The overall format effect was not significant ($p = 0.303$), and the format-by-rest-time interaction did not reach significance ($p = 0.0508$). Thus, increasing the interval between plating and stimulation altered reporter output in both assay-ready and cultured cells.

Together, these experiments show that assay-ready THP-1 cells retain robust inducible NF-κB responsiveness despite ongoing molecular remodeling. The broad concentration-response and temporal response patterns were conserved, while a reproducible difference in intermediate early activation and a strong dependence on post-plating timing demonstrate that functional output remains sensitive to the assay window.

Discussion

The central finding of this study is that cryopreserved THP-1 cells do not occupy a single post-thaw state but progress through an organized molecular transition. This response was most pronounced at the transcript level, where substantial remodeling developed during the first several hours after thaw, but temporal organization was also evident at the pathway and protein levels. Broad transcriptional responses are well established in monocytic systems exposed to acute stress or inflammatory stimulation[10] and in THP-1 cells undergoing differentiation[11], while cold-chain manipulation can itself alter gene expression in mononuclear cells[12]. Cryopreservation-associated proteomic changes have also been reported in myeloid cell models[13]. The present study extends this work by resolving how molecular state changes across post-thaw time rather than treating cryopreservation as a single before-versus-after perturbation.

Hallmark analysis showed that post-thaw remodeling proceeded through temporally distinct inflammatory, stress, proliferative, and metabolic programs rather than a monotonic return toward the immediate post-thaw state. The broader early transcriptional response and narrower later proteomic response are consistent with the differing kinetics of transcription, translation, degradation, and persistence of pre-existing proteins[14,15], although the experimental design does not define a fixed transcript-to-protein delay. Targeted cryostress analysis further distinguished conserved from context-sensitive responses, with STD and AR responses remaining highly correlated across the full marker panel. ANXA1 and ANXA2 represented one of the clearest conserved responses, showing strong transcriptional induction and among the largest later increases in protein abundance. Annexins are calcium-regulated membrane-binding proteins involved in membrane organization and plasma-membrane resealing following injury[16]. Because cryopreservation imposes osmotic and membrane stress that may persist despite gross membrane integrity[17], the

consistency of the annexin response across formats and molecular layers supports membrane remodeling as a prominent component of the post-thaw response.

Other modules were more context sensitive. Proteostasis markers including HSPA1A, HSPA1B, DNAJB1, and HSPA5 generally showed stronger transcriptional engagement in AR cells, whereas DDIT4 and HMOX1 differed in the magnitude or persistence of metabolic and oxidative stress responses. Cryopreservation-associated heat-shock responses, including HSPA1A and HSPA1B induction, have been reported in other human systems[18]. However, later protein remodeling was dominated less by proteostasis changes than by shared annexin and antioxidant-associated responses. Thus, STD and AR cells appear to engage a strongly overlapping stress response while differing in the weighting and persistence of selected components.

Cryopreservation-related stress also should not be equated directly with irreversible injury. Oxidative stress, unfolded-protein responses, apoptosis-associated signaling, and other stress pathways continue to evolve after thaw, and intervention during the post-thaw period can alter subsequent recovery in hematopoietic cells[19]. The mixed behavior of proteostasis, antioxidant, metabolic, survival, and protein-clearance markers observed here is more consistent with an adaptive and dynamically changing response than with a uniform cell-death program.

The complementary experimental designs support a contribution of upstream cellular context to the phenotype observed after thaw. The transcriptomic STD and AR preparations were generated from independently prepared starting populations, and hundreds of differences were apparent immediately after thaw. These differences cannot be assigned uniquely to production state or preservation history, but their presence at the earliest measured time point is consistent with distinct biological states entering the post-thaw interval. Those differences were not simply maintained unchanged: individual transcripts continued to turn over across 2 and 8 h while the two preparations followed strongly concordant response directions.

One notable component of this separation was the persistent relative enrichment of inflammatory programs in AR cells, including TNFα signaling via NF-κB, inflammatory response, and interferon-associated pathways. Upstream culture conditions, including media formulation and cell density, can substantially alter transcriptional profiles[20], and independently propagated populations of the same cell line can acquire biologically relevant genetic and transcriptional differences[21]. Immune-cell state at the time of cryopreservation can also influence subsequent proliferation and function[22]. The present data are therefore consistent with persistence of aspects of upstream biological state after cryopreservation.

The proteomic experiment provides an important counterpoint because STD and AR cells were separated from a common harvest. Under this design, direct protein-abundance differences between formats were minimal throughout the measured interval, even though both populations underwent substantial time-dependent remodeling relative to their reference states. The smaller format effect observed when pre-freeze state was shared supports the interpretation that upstream production context contributes to the larger separation seen between independently produced transcriptomic preparations. At the same time, the strong concordance across both experimental designs indicates that differences in cellular context can alter the magnitude or persistence of selected responses without redirecting cells into fundamentally different post-thaw programs.

Reference choice also influences the apparent scale of these effects. The 6-day transcriptomic reference represents a later cultured state and therefore differs from acute post-thaw cells in growth state, density, and culture adaptation in addition to any residual cryopreservation effect. Similarly, the proteomic CC-72 h reference captures continued culture rather than an invariant pre-freeze baseline. These comparators are useful for contextualizing different stages of the experimental system, but differential feature counts relative to them should not be interpreted as quantitative measures of cryoinjury. The more consistent finding across analyses is the organization of the response: post-thaw time strongly structures both datasets, STD and AR cells generally change in the same direction, and cellular context modifies selected features within that shared trajectory.

This distinction is relevant to cell banking because a cryopreserved vial contains a particular cellular population rather than an abstract cell-line identity. Passage history, density, growth phase, harvest state, and upstream handling can therefore contribute to the biological state ultimately delivered after thaw. For assay-ready workflows, control of the post-thaw input begins with control of the population entering cryopreservation.

The broader transcriptomic response relative to the proteomic response does not imply that early transcriptional remodeling lacks biological relevance. RNA abundance, total protein abundance, and cellular function report different dimensions of cellular state and need not change synchronously. Transcriptional responses can occur rapidly while protein-abundance changes emerge more gradually through synthesis and turnover[14,15], and total abundance does not capture post-translational regulation or protein localization[23]. Consistent with this temporal layering, broad transcriptional changes appeared within the first 8 h, whereas protein-level remodeling was more restricted and developed over 24–72 h. The molecular layers should therefore be viewed as complementary measurements of a changing cellular state rather than as a continuous transcript-to-protein kinetic series.

The NF-κB reporter experiments extend this distinction to assay-relevant function. Assay-ready cells retained robust inducible responses across LPS concentration and stimulation-duration experiments, with broadly conserved concentration-response behavior and stimulation kinetics. Although cultured cells showed greater activity at selected early time points, this difference was localized within an otherwise similar response. Thus, molecular nonequivalence did not preclude robust inducible NF-κB responsiveness.

The inflammatory enrichment observed in the AR transcriptome is notable in this context because assay-ready cells entered use with immune-response programs already shifted relative to STD cells while retaining substantial capacity for further stimulus-induced NF-κB activation. The functional data therefore reinforce a distinction between molecular state and inducible signaling capacity: differences in baseline molecular state can coexist with preservation of the broader response program.

Post-plating timing was also an important determinant of functional output. Rest time altered reporter magnitude in both assay-ready and non-frozen cultured cells, indicating that the effect cannot be attributed solely to cryopreservation recovery. Adaptation to the assay environment, including changes in density and media exposure, may contribute to these post-plating effects. The measured phenotype therefore reflects not only preservation history but also the biological state established during assay adaptation.

This observation has a direct implication for the concept of assay readiness. Immediate post-thaw viability alone does not establish that cells are biologically static or equivalent to a continuously cultured reference. Membrane integrity can fail to detect subcellular changes that influence later recovery[17], and short-term viability can overestimate cryopreservation success when subsequent recovery and delayed cell loss are not considered[24]. Conversely, complete molecular equivalence to a cultured reference is not necessarily required for a useful assay. Previous work developing assay-ready cryopreserved cell systems has similarly evaluated combinations of recovery, proliferation, metabolism, apoptosis, cell-cycle behavior, and application-specific function rather than relying on a single viability measurement[25].

The present data add a temporal dimension to this framework. Post-thaw and post-plating time should be treated as controlled experimental variables because functional output can change substantially during the intended use period. For assay-ready systems, the relevant criterion is therefore reproducible functional performance within a defined biological window rather than immediate viability or complete molecular equivalence to a continuously cultured control.

Several limitations should be considered. The transcriptomic and proteomic datasets were deliberately generated using complementary experimental designs and therefore

differ in starting material, reference state, and sampling interval. These differences enable distinct comparisons, particularly the contrast between independently produced transcriptomic inputs and the shared proteomic harvest, but they prevent direct quantitative alignment of RNA and protein kinetics. The functional reporter experiments were performed in a related THP-1 reporter system rather than the cells used for omics profiling, so molecular and functional measurements should be interpreted as complementary levels of evidence rather than a continuous mechanistic series. The targeted cryostress analysis identifies response patterns but does not directly measure membrane repair, autophagic flux, protein activation, or pathway activity. Finally, the current experiments do not establish lot-to-lot or interlaboratory reproducibility across independent manufacturing campaigns.

The combined data support a model in which cryopreserved THP-1 cells pass through an organized post-thaw transition containing both highly conserved responses and components whose magnitude or persistence is sensitive to cellular and preservation context. The state present at the time of freezing remains relevant after thaw, while transcript abundance, protein abundance, and inducible function resolve different aspects of the subsequent trajectory. Substantial molecular remodeling can therefore coexist with preserved NF-κB responsiveness. For assay-ready systems, both the biological state entering preservation and the timing of experimental use contribute to the phenotype delivered to an assay.

Methods

Cell culture, preservation, and experimental design

THP-1 cells were maintained in RPMI-1640 medium (ATCC® 30-2001™) supplemented with 10% fetal bovine serum (FBS; ATCC® 30-2020™) at densities between 0.1–1.5 × 10^6 cells/mL. Cells were cultured in a humidified incubator at 37°C with 5% CO_2 according to ATCC-recommended procedures.

THP-1 cells and derivative preparations used in this study were obtained directly from ATCC (Manassas, VA, USA), including STD THP-1 cells (ATCC® TIB-202™), AR THP-1 cells (ATCC® TIB-202-AR™), and THP-1 NF-κB-Luc2 reporter cells (ATCC® TIB-202-NFκB-LUC2™). Cell identity was confirmed as part of ATCC lot-release quality control using short tandem repeat profiling, with results consistent with the established THP-1 identity profile. Authentication and mycoplasma testing were performed as part of lot-release testing before experimental use.

For transcriptomic analysis, STD and AR THP-1 preparations generated from independently prepared starting pools were evaluated at 0, 2, and 8 h post-thaw. An additional STD-derived culture maintained for 6 days after thaw served as the recovered

reference. The AR 2-h group and 6-day reference each contained five biological replicates; all other transcriptomic groups contained three.

For proteomic analysis, a single pooled THP-1 culture was divided among STD and AR preservation conditions and a non-frozen continued-culture arm. The STD cryoprotectant medium consisted of a complete growth medium supplemented with 5% dimethyl sulfoxide, whereas the AR formulation was proprietary. Samples were collected at harvest, after a 2-h room-temperature cryoprotectant-medium hold, immediately after thaw, and at 24 and 72 h post-thaw. The non-frozen arm was maintained for 72 h after harvest and designated CC-72 h. Ten proteomic groups were analyzed in biological triplicate.

Frozen preparations contained 5–10 × 10^6 cells and were processed using a Thermo Scientific CryoMed controlled-rate freezer before storage in the vapor phase of liquid nitrogen. After thawing, cell suspensions were diluted 1:9 in complete growth medium, centrifuged at 200 × *g* at 4°C, and resuspended in fresh medium before culture or sample collection.

RNA isolation, library preparation, and sequencing

Total RNA was extracted using the RNeasy Mini QIAcube Kit on a QIAcube automated system (QIAGEN). Concentration and purity were assessed by the Thermo Fisher Scientific NanoDrop spectrophotometer, with acceptable A260/A280 ratios of 1.8–2.2. RNA integrity was evaluated using an Agilent TapeStation, and samples with an RNA integrity number ≥ 6.5 were advanced to library preparation.

RNA-seq libraries were prepared using an Eppendorf epMotion 5075 liquid handler with the Illumina Stranded mRNA Prep, Ligation kit. Libraries were quantified using the Qubit double-stranded DNA High Sensitivity Assay and evaluated using an Agilent 4200 TapeStation with D5000 ScreenTape. Sequencing was performed on an Illumina NextSeq 2000 sequencer using a P3 200-cycle reagent kit.

RNA-seq processing, quality control, and statistical analysis

Raw paired-end reads were processed using CLC Genomics Workbench v25 (QIAGEN Digital Insights). Reads were trimmed at a minimum quality score of Q30, adapter read-through, and 3′ poly-G sequences were removed and reads shorter than 50 bp were discarded. Processed reads were aligned to the hg38 human reference genome and corresponding Ensembl annotation using the stranded CLC bulk RNA-seq workflow. Each biological replicate was required to contain at least 18 million mapped reads.

Gene-level raw counts were exported to R. Duplicate gene identifiers were collapsed by summing counts, genes with zero total counts were removed, and a condition-based filter retained genes with mean counts per million >0.2 in at least one experimental

group. Differential expression was analyzed using DESeq2[26], with each preservation-format and time-point combination represented as a separate condition level. The standard DESeq2 workflow was used for normalization, dispersion estimation, Wald testing, independent filtering, Cook's-distance handling, and Benjamini–Hochberg adjustment. Differentially expressed genes were defined by adjusted $p < 0.05$ and $|\log_2$ fold change$| > 1$.

For quality control and principal component analysis (PCA), genes with at least 10 raw counts in more than three samples were retained. Variance stabilized expression values were generated using DESeq2 with transformation performed blind to experimental conditions. Standard sample-level quality-control metrics were examined for replicate consistency. PCA was performed using the complete filtered matrix with feature centering and without variance scaling.

Proteomic sample preparation and tandem mass tag (TMT) analysis

Thirty cell pellets representing 10 experimental groups in biological triplicate were submitted to Poochon Scientific for tandem mass tag-based quantitative proteomic analysis. Pellets were lysed in 50 mM triethylammonium bicarbonate (pH 8.0) containing 2% sodium dodecyl sulfate. Lysates were sonicated and clarified by centrifugation at 15,000 × *g* for 10 min at 4°C. Protein concentration was measured using a reducing-agent-compatible bicinchoninic acid assay.

Aliquots containing 100 µg of protein were reduced with tris(2-carboxyethyl) phosphine, alkylated with iodoacetamide, and digested with trypsin for 16 h at 37°C. Peptides were labeled using two TMT 18-plex reagent sets. The same pooled master-mix reference was included in both TMT plexes to support normalization across plexes. Labeled peptides were fractionated into 24 fractions per set by high-pH reverse-phase liquid chromatography.

Fractions were analyzed using a Thermo Scientific Orbitrap Exploris 240 mass spectrometer coupled to an Ultimate 3000 RSLCnano system. Peptides were separated on a 25-cm C18 column using a 110-min gradient from 3% to 36% acetonitrile in 0.1% formic acid. Data-dependent acquisition included full MS scans from m/z 350 to 1,800 followed by higher-energy collisional dissociation of MS/MS of the 20 most abundant multiply charged precursors, with a 20-s dynamic exclusion.

Raw files were processed using Proteome Discoverer v2.5 and searched against the UniProtKB human protein database using SEQUEST with Percolator validation. False-discovery rates of 1% were applied at the peptide and protein levels. Protein abundance ratios were calculated from summed TMT reporter-ion intensities relative to the corresponding reference channel, normalized within each TMT run to the shared reference, and median-centered across samples.

Proteomic quality control and statistical analysis

For proteomic PCA, normalized abundance values were winsorized independently within each sample at the 1st and 99th percentiles and median-centered. This processing was used only for PCA and was not applied to differential-abundance or pathway analyses. One harvest replicate was excluded from the displayed PCA because its extreme position compressed the visualization of the remaining samples; it was retained in all differential-abundance and pathway analyses.

Differential abundance was analyzed using limma[27] on the run-normalized, median-centered abundance matrix. The matrix contained complete values for 6,285 protein groups. A no-intercept condition model was fitted, predefined contrasts were evaluated using empirical Bayes moderation, and p values were adjusted using the Benjamini–Hochberg method. Differentially abundant proteins were defined by adjusted $p < 0.05$ and $|\log_2 \text{fold change}| > 0.58$, corresponding to a 1.5-fold difference.

Concordance analysis

Concordance between STD and AR responses was evaluated at matched time points using feature-level $\log_2$ fold changes relative to the corresponding reference condition. Features meeting the predefined differential expression or abundance criteria in at least one format were included and classified as significant in both formats, STD only, or AR only.

Directional concordance was calculated as the percentage of included features with $\log_2$ fold changes of the same sign in STD and AR. R^2 was calculated as the squared Pearson correlation coefficient between paired $\log_2$ fold-change values.

Variance partitioning

Feature-level variance was partitioned separately for the transcriptomic and proteomic datasets using factorial models containing time, condition, and their interaction, with condition representing STD versus AR. Transcriptomic analysis included matched STD and AR samples at 0, 2, and 8 h post-thaw; genes with counts per million (CPM) ≥1 in at least three samples were transformed as $\log_2(\text{CPM} + 0.5)$, and nonfinite or zero-variance features were removed. The 6-day reference was excluded. Proteomic analysis included matched STD and AR samples from the 2-h cryoprotectant-medium hold and 0-, 24-, and 72-h post-thaw groups; Harvest and CC-72 h were excluded.

Variance contributions were estimated using a hierarchy-preserving, order-independent decomposition of model R^2. The interaction component was defined as the incremental variance explained by the full time × condition model beyond the additive time + condition model. Variance explained by the additive model was allocated between time and condition using Shapley averaging of their incremental contributions across both

possible entry orders. Residual variance was defined as one minus the full-model R^2. Component fractions were summarized as the median across features, with 95% confidence intervals calculated from 2,000 feature-level bootstrap resamples.

Hallmark gene set enrichment analysis

Transcriptomic and proteomic differential-analysis results were analyzed separately by ranked-list gene set enrichment analysis[28]. Human Hallmark gene sets were obtained from the Molecular Signatures Database (MSigDB)[29] using the msigdbr R package, and enrichment was performed using fgsea.

Genes were ranked by the signed DESeq2 Wald statistic and proteins by the moderated limma *t* statistic. Gene and protein identifiers were mapped to human gene symbols and collapsed to one ranked entry. Sets containing 15–500 members were evaluated. Transcriptomic pathways were considered significant at adjusted $p < 0.01$, whereas proteomic pathways were considered significant at adjusted $p < 0.05$. No normalized enrichment score threshold was applied. Adjusted *p* values were calculated using the Benjamini-Hochberg method.

For temporal pathway analysis, enrichment was evaluated separately within STD and AR THP-1 cells. Transcriptomic comparisons included 2 h versus 0 h, 8 h versus 2 h, and 8 h versus 0 h, while proteomic comparisons included 24 h versus 0 h, 72 h versus 24 h, and 72 h versus 0 h. Positive normalized enrichment score (NES) values indicate enrichment at the later time point of each comparison and negative values indicate enrichment at the earlier time point. For visualization, pathways meeting the respective significance criteria were prioritized based on the largest absolute NES and greatest temporal variability across the displayed comparisons.

For temporal summary plots, STD and AR NES values were averaged for each pathway and comparison. Early-versus-late plots compared mean NES for 2 h versus 0 h with 8 h versus 2 h for transcriptomics and mean NES for 24 h versus 0 h with 72 h versus 24 h for proteomics. For cross-omic comparison, Hallmark pathways represented in both displayed pathway sets were evaluated by comparing mean STD/AR NES at 8 h versus 0 h for RNA with mean STD/AR NES at 24 h versus 0 h for protein. This comparison was used descriptively to evaluate agreement in enrichment direction across molecular layers.

Targeted cryostress marker analysis

A literature-informed panel of 37 markers was assembled to examine molecular processes associated with cryopreservation stress and post-thaw recovery. Markers represented eight functional categories: cold shock, rewarming/proteostasis, endoplasmic-reticulum stress and integrated stress response, oxidative/metabolic stress, apoptosis/survival, cell-cycle/DNA stress, osmotic/membrane regulation, and

autophagy/protein clearance. The complete marker list, functional classifications, rationale for inclusion, and supporting literature are provided in Supplementary Table S1. Markers were evaluated as a targeted descriptive panel irrespective of genome-wide differential-expression significance.

For transcriptomic analysis, descriptive log2 fold changes were calculated from normalized RNA abundance. The 0-h AR-versus-STD comparison was used to characterize differences in the molecular state entering post-thaw recovery. Temporal responses were then normalized independently within each format, with STD 2 h and 8 h compared with STD 0 h and AR 2 h and 8 h compared with AR 0 h. This within-format normalization was used so that temporal responses were not driven by the initial difference between the independently prepared STD and AR transcriptomic populations.

The similarity of the STD and AR transcriptional responses was evaluated across all 37 markers using Pearson correlation of the within-format log2 fold changes at 2 and 8 h. These correlations describe agreement in the magnitude and direction of the targeted marker response rather than statistical significance of individual markers.

For proteomic analysis, markers were considered detected when retained in the processed TMT abundance matrix. Twenty-one of the 37 targeted markers were detected. Protein changes at 24 and 72 h were calculated relative to the mean abundance of the shared harvest pool and expressed as log2 fold change. HSPA1A was not detected in the proteomic dataset; HSPA1B is shown as the detected inducible HSP70-family correlate. The targeted RNA and protein analyses were used to describe complementary early and later molecular responses and were not treated as a continuous transcript-to-protein kinetic series.

NF-κB luciferase reporter assay

THP-1 NF-κB-Luc2 reporter cells (ATCC® TIB-202-NFκB-LUC2™) were expanded under standard culture conditions and used to generate assay-ready preparations. Reporter activity was compared with non-frozen cultured cells from the same model collected at the culture state corresponding to the assay-ready harvest.

Cells were seeded at 20,000 cells per well in tissue-culture-treated 96-well plates containing RPMI-1640 medium supplemented with 10% FBS. The concentration-response experiment comprised three independent biological experiments, with one measurement collected per condition in each experiment. Stimulation-duration and post-plating rest-time experiments comprised four independent biological experiments generated from separate cultures and independently prepared assay-ready materials, with each condition measured in technical triplicate. Matched unstimulated controls were included in each experiment.

For concentration-response analysis, cells were stimulated immediately after plating with 0.0016, 0.008, 0.04, 0.2, 1, or 5 µg/mL Escherichia coli O111 lipopolysaccharide (LPS; Sigma-Aldrich, L2630) for 3 h. Stimulation kinetics were evaluated using 1 µg/mL LPS for 0, 1, 2, 3, 4, 6, 8, or 24 h. For post-plating rest-time analysis, cells were rested for 0, 3, 5, or 24 h before stimulation with 1 µg/mL LPS for 3 h.

Luciferase activity was measured using the Bright-Glo Luciferase Assay System and a GloMax plate reader according to the manufacturer's procedures (Promega). Reporter activity was expressed as fold induction relative to the corresponding unstimulated condition. For stimulation-duration and rest-time experiments, technical triplicates were averaged within each biological experiment before analysis. Data are presented as mean ± standard deviation (SD) across independent biological experiments.

Statistical Analyses

Biological replicates represent independently prepared cultures or cell preparations as defined for each experiment. Transcriptomic groups contained three biological replicates, except the AR 2-h group and 6-day recovered reference, which contained five. Proteomic groups were analyzed in biological triplicate. The NF-κB concentration-response experiment comprised three independent biological experiments, whereas stimulation-duration and post-plating rest-time experiments comprised four independent biological experiments. For the latter experiments, technical triplicates were averaged within each biological experiment before statistical analysis.

RNA-seq differential expression was analyzed using DESeq2 with Wald testing and Benjamini–Hochberg correction for multiple comparisons; differentially expressed genes were defined by adjusted $p < 0.05$ and |log2 fold change| > 1. Differential protein abundance was analyzed using limma with empirical Bayes moderation and Benjamini–Hochberg correction; differentially abundant proteins were defined by adjusted $p < 0.05$ and $|\log_2 \text{fold change}| > 0.58$. Hallmark gene-set enrichment was performed using fgsea with Benjamini–Hochberg correction, with significance thresholds of adjusted $p < 0.01$ for transcriptomic analyses and adjusted $p < 0.05$ for proteomic analyses. Pearson correlation was used for concordance analyses. Reporter-assay data are presented as mean ± SD across independent biological experiments. Statistical tests, sample sizes, and exact p values are reported in the corresponding Methods, figure legends, or Results.

NF-κB concentration-response, stimulation-duration, and post-plating rest-time experiments were analyzed using two-factor repeated-measures ANOVA with cell format, the corresponding experimental variable, and their interaction included in the model and biological experiment treated as the repeated unit. Greenhouse–Geisser correction was applied to effects involving multi-level within-experiment factors. Baseline values fixed at a fold induction of 1 by normalization, including the 0 µg/mL

concentration-response control and 0-h stimulation-duration condition, were excluded from inferential models. Planned paired comparisons between formats or time points were performed on biological-experiment-level values and adjusted for multiple comparisons within each comparison family using the Holm method. All analyses were performed on the untransformed fold-induction values. All statistical tests were two-sided, with $p < 0.05$ considered statistically significant.

References

1. Baust, J. G., Snyder, K. K., Van Buskirk, R. & Baust, J. M. Integrating Molecular Control to Improve Cryopreservation Outcome. *Biopreserv Biobank* **15**, 134–141 (2017).
2. Stacey, G. N. & Masters, J. R. Cryopreservation and banking of mammalian cell lines. *Nat Protoc* **3**, 1981–1989 (2008).
3. Fuller, B. J. Cryoprotectants: the essential antifreezes to protect life in the frozen state. *Cryo Letters* **25**, 375–388 (2004).
4. Baust, J. M., Corwin, W., Snyder, K. K., Van Buskirk, R. & Baust, J. G. Cryopreservation: Evolution of Molecular Based Strategies. *Adv Exp Med Biol* **951**, 13–29 (2016).
5. Xu, X. *et al*. The roles of apoptotic pathways in the low recovery rate after cryopreservation of dissociated human embryonic stem cells. *Biotechnol Prog* **26**, 827–837 (2010).
6. Meneghel, J., Kilbride, P. & Morris, G. J. Cryopreservation as a Key Element in the Successful Delivery of Cell-Based Therapies-A Review. *Front Med (Lausanne)* **7**, 592242 (2020).
7. Tsuchiya, S. *et al*. Induction of maturation in cultured human monocytic leukemia cells by a phorbol diester. *Cancer Res* **42**, 1530–1536 (1982).
8. Chanput, W., Mes, J. J. & Wichers, H. J. THP-1 cell line: an in vitro cell model for immune modulation approach. *Int Immunopharmacol* **23**, 37–45 (2014).

9. Singh, A. P., Wax, N., Duncan, J., Fernandes, A. S. & Jacobs, J. L. Genomic discovery of EF-24 targets unveils antitumorigenic mechanisms in leukemia cells. *PLoS One* **20**, e0330906 (2025).
10. Wong, H. R., Odoms, K. & Sakthivel, B. Divergence of canonical danger signals: The genome-level expression patterns of human mononuclear cells subjected to heat shock or lipopolysaccharide. *BMC Immunol* **9**, 24 (2008).
11. Zeng, C. *et al.* Pathways related to PMA-differentiated THP1 human monocytic leukemia cells revealed by RNA-Seq. *Sci China Life Sci* **58**, 1282–1287 (2015).
12. Yang, J. *et al.* The effects of storage temperature on PBMC gene expression. *BMC Immunol* **17**, 6 (2016).
13. Al-Otaibi, N. A. S., Cassoli, J. S., Martins-de-Souza, D., Slater, N. K. H. & Rahmoune, H. Human leukemia cells (HL-60) proteomic and biological signatures underpinning cryo-damage are differentially modulated by novel cryo-additives. *Gigascience* **8**, giy155 (2019).
14. Jovanovic, M. *et al.* Dynamic profiling of the protein life cycle in response to pathogens. *Science* **347**, 1259038 (2015).
15. Cheng, Z. *et al.* Differential dynamics of the mammalian mRNA and protein expression response to misfolding stress. *Mol Syst Biol* **12**, 855 (2016).
16. Koerdt, S. N. & Gerke, V. Annexin A2 is involved in Ca2+-dependent plasma membrane repair in primary human endothelial cells. *Biochim Biophys Acta Mol Cell Res* **1864**, 1046–1053 (2017).

17. Tchir, J. & Acker, J. P. Mitochondria and membrane cryoinjury in micropatterned cells: effects of cell-cell interactions. *Cryobiology* **61**, 100–107 (2010).
18. Wu, S. Z. *et al.* Cryopreservation of human cancers conserves tumour heterogeneity for single-cell multi-omics analysis. *Genome Med* **13**, 81 (2021).
19. Baust, J. M., Snyder, K. K., Van Buskirk, R. G. & Baust, J. G. Assessment of the Impact of Post-Thaw Stress Pathway Modulation on Cell Recovery following Cryopreservation in a Hematopoietic Progenitor Cell Model. *Cells* **11**, 278 (2022).
20. Kim, S. W., Kim, S.-J., Langley, R. R. & Fidler, I. J. Modulation of the cancer cell transcriptome by culture media formulations and cell density. *Int J Oncol* **46**, 2067–2075 (2015).
21. Ben-David, U. *et al.* Genetic and transcriptional evolution alters cancer cell line drug response. *Nature* **560**, 325–330 (2018).
22. Luo, Y. *et al.* The state of T cells before cryopreservation: Effects on post-thaw proliferation and function. *Cryobiology* **79**, 65–70 (2017).
23. Mulvey, C. M. *et al.* Spatiotemporal proteomic profiling of the pro-inflammatory response to lipopolysaccharide in the THP-1 human leukaemia cell line. *Nat Commun* **12**, 5773 (2021).
24. Murray, K. A. & Gibson, M. I. Post-Thaw Culture and Measurement of Total Cell Recovery Is Crucial in the Evaluation of New Macromolecular Cryoprotectants. *Biomacromolecules* **21**, 2864–2873 (2020).

25. Tomás, R. M. F., Bissoyi, A., Congdon, T. R. & Gibson, M. I. Assay-ready Cryopreserved Cell Monolayers Enabled by Macromolecular Cryoprotectants. *Biomacromolecules* **23**, 3948–3959 (2022).
26. Love, M. I., Huber, W. & Anders, S. Moderated estimation of fold change and dispersion for RNA-seq data with DESeq2. *Genome Biol* **15**, 550 (2014).
27. Ritchie, M. E. *et al.* limma powers differential expression analyses for RNA-sequencing and microarray studies. *Nucleic Acids Res* **43**, e47 (2015).
28. Subramanian, A. *et al.* Gene set enrichment analysis: a knowledge-based approach for interpreting genome-wide expression profiles. *Proc Natl Acad Sci U S A* **102**, 15545–15550 (2005).
29. Liberzon, A. *et al.* The Molecular Signatures Database (MSigDB) hallmark gene set collection. *Cell Syst* **1**, 417–425 (2015).

Data availability

Source data underlying the main and supplementary figures are provided with this paper. Mass-spectrometry proteomics data generated in this study have been deposited with the ProteomeXchange Consortium through the PRIDE repository under accession PXD084700 and are currently available through private reviewer access. Reviewer access is available at https://www.ebi.ac.uk/pride/login using accession PXD084700 and reviewer token b0WIbWhYaVQh. Submission of the RNA-sequencing data to the NCBI Gene Expression Omnibus (GEO) is in progress, and the accession number will be provided when available. Additional datasets generated and analyzed during the current study are available from the corresponding authors upon reasonable request.

Code availability

Custom code used for the order-independent variance-partitioning analysis is available from the corresponding authors upon reasonable request.

Acknowledgements

We thank Utsav Sharma for discussions that helped inform the initial application context and motivation for this study.

Funding

This work was supported by internal ATCC resources.

Author contributions

L.U. and A.P.S. contributed equally to this work and were responsible for conceptualization, methodology, investigation, formal analysis, data curation, visualization, project administration, and writing of the original draft. J.M. contributed to methodology, investigation, and data collection for the functional NF-κB experiments. N.W. and S.K. contributed to RNA-sequencing and data processing. J.L.J. and N.C. contributed to conceptualization, supervision, resources, and scientific direction. All authors contributed to review and editing of the manuscript and approved the final version.

Competing interests

All authors are employees of ATCC. ATCC develops and distributes the THP-1 cell products evaluated in this study. The authors declare no other competing interests.

Figures and legends

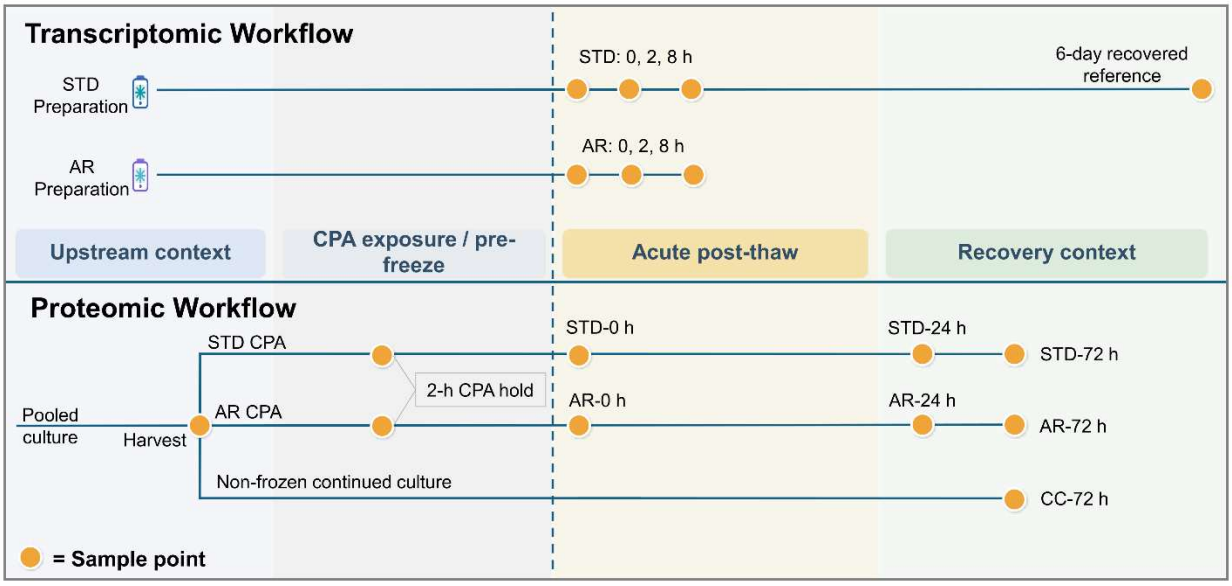


Fig. 1 | Experimental design for transcriptomic and proteomic profiling of post-thaw THP-1 cells. Transcriptomic profiling compared independently produced standard-vial (STD) and assay-ready (AR) preparations at 0, 2, and 8 h post-thaw with a 6-day STD-derived recovered reference. Proteomic profiling followed a shared harvest through STD and AR cryoprotectant-medium hold, 0-, 24-, and 72-h post-thaw states, with a non-frozen continued-culture reference at 72 h (CC-72 h). Circles denote sampled states; shading distinguishes upstream, pre-freeze, acute post-thaw, and later culture intervals.

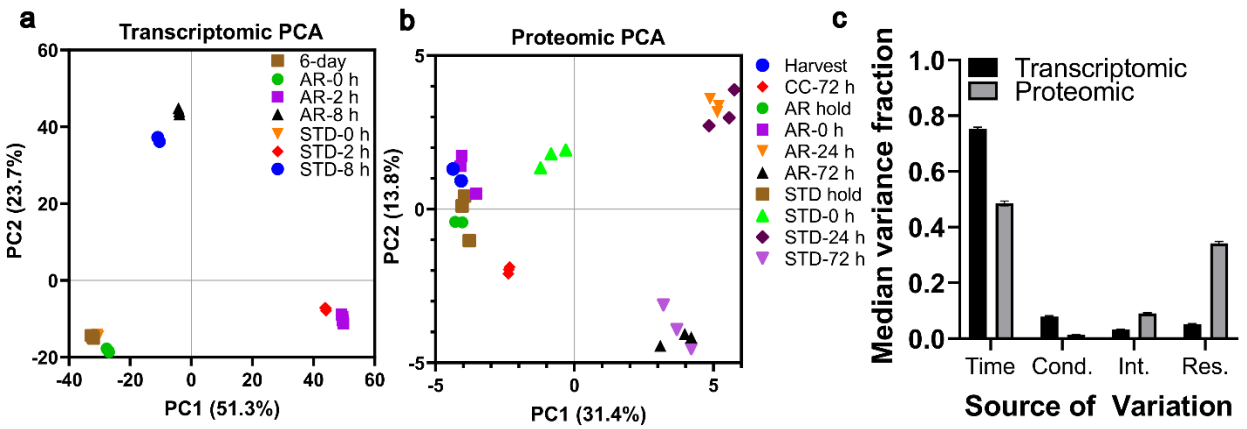


Fig. 2 | Global transcriptomic and proteomic structure across post-thaw progression. a, Principal component analysis (PCA) of RNA-seq profiles from STD and AR cells at 0, 2, and 8 h and the 6-day recovered reference. b, PCA of normalized protein abundance across Harvest, 2-h hold, 0-, 24-, and 72-h post-thaw, and CC-72 h states. Points represent biological replicates. RNA-seq: n = 3 per group except AR 2 h and 6-day reference, n = 5. Proteomics: n = 3 per group; one Harvest replicate was excluded from PCA visualization only (displayed n = 2). c, Order-independent variance partitioning of matched STD and AR samples. Bars show median variance fractions across 13,130 genes or 6,285 proteins; error bars are 95% bootstrap confidence intervals from 2,000 feature-level resamples.

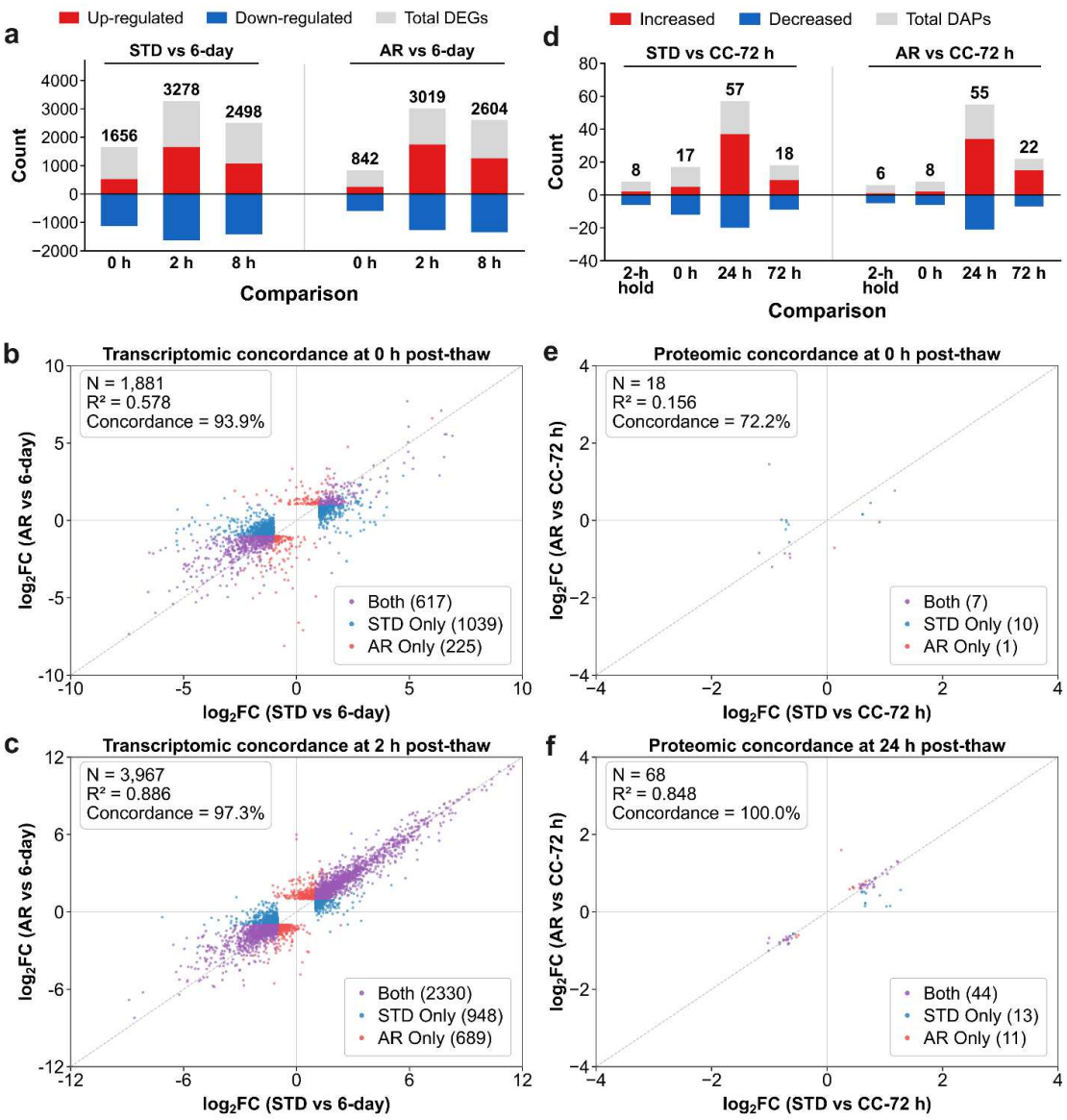
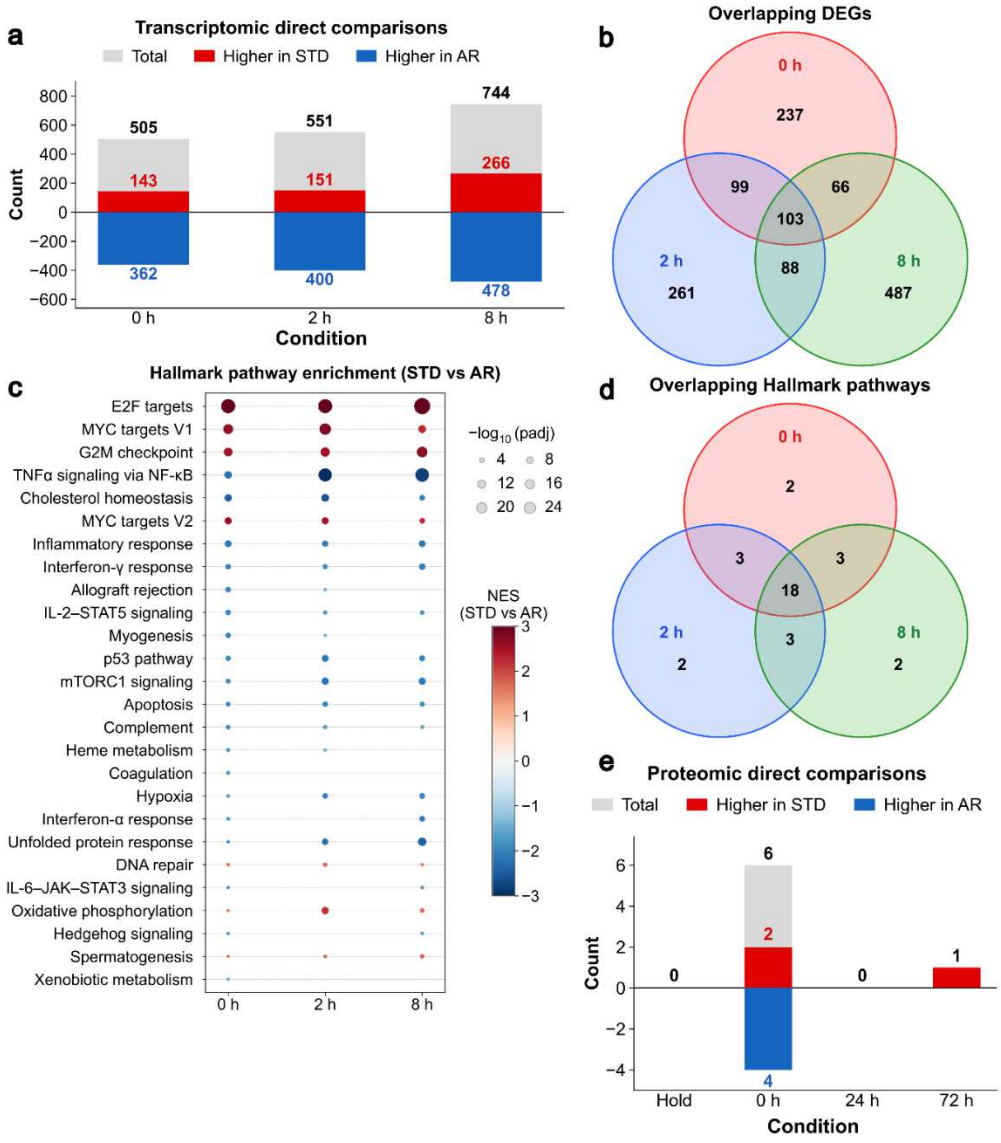


Fig. 3 | Differential feature burden and cross-format response concordance. a, Differentially expressed genes (DEGs) in STD and AR cells at 0, 2, and 8 h relative to the 6-day recovered reference (adjusted $p < 0.05$, $|\log_2 \text{fold change}| > 1$). b,c, STD-versus-AR concordance of transcriptomic responses at 0 and 2 h. d, Differentially abundant proteins (DAPs) relative to CC-72 h following the 2-h hold and at 0, 24, and 72 h (adjusted $p < 0.05$, $|\log_2 \text{fold change}| > 0.58$). e,f, Proteomic response concordance at 0 and 24 h. Features meeting significance criteria in either format are shown; colors denote significance in both formats, STD only, or AR only. R^2 is the squared Pearson correlation coefficient; concordance is the percentage changing in the same direction. Dashed diagonals denote identity. RNA-seq: n = 3 biological replicates per group except AR 2 h and 6-day reference, n = 5; proteomics: n = 3 per group.



822

823 **Fig. 4 | Direct molecular differences between STD and AR THP-1 cells.**
824 Comparisons are oriented as STD versus AR; positive values indicate higher
825 expression, abundance, or enrichment in STD. a, DEGs between formats at 0, 2, and 8
826 h (adjusted $p < 0.05$, $|\log_2$ fold change$| > 1$). b, Overlap of DEGs across time points. c,
827 Hallmark pathway enrichment across matched time points; bubble color denotes
828 normalized enrichment score (NES) and size denotes $-\log_{10}$(adjusted p). Displayed
829 pathways are those significant at 0 h (adjusted $p < 0.01$), shown across all three
830 matched time points. d, Overlap of significant Hallmark pathways (adjusted $p < 0.01$). e,
831 DAPs between formats following the 2-h hold and at 0, 24, and 72 h (adjusted $p < 0.05$,
832 $|\log_2$ fold change$| > 0.58$). In a,e, features higher in AR are plotted below zero; counts
833 are absolute. RNA-seq: n = 3 biological replicates per group except AR 2 h, n = 5;
834 proteomics: n = 3 per group.

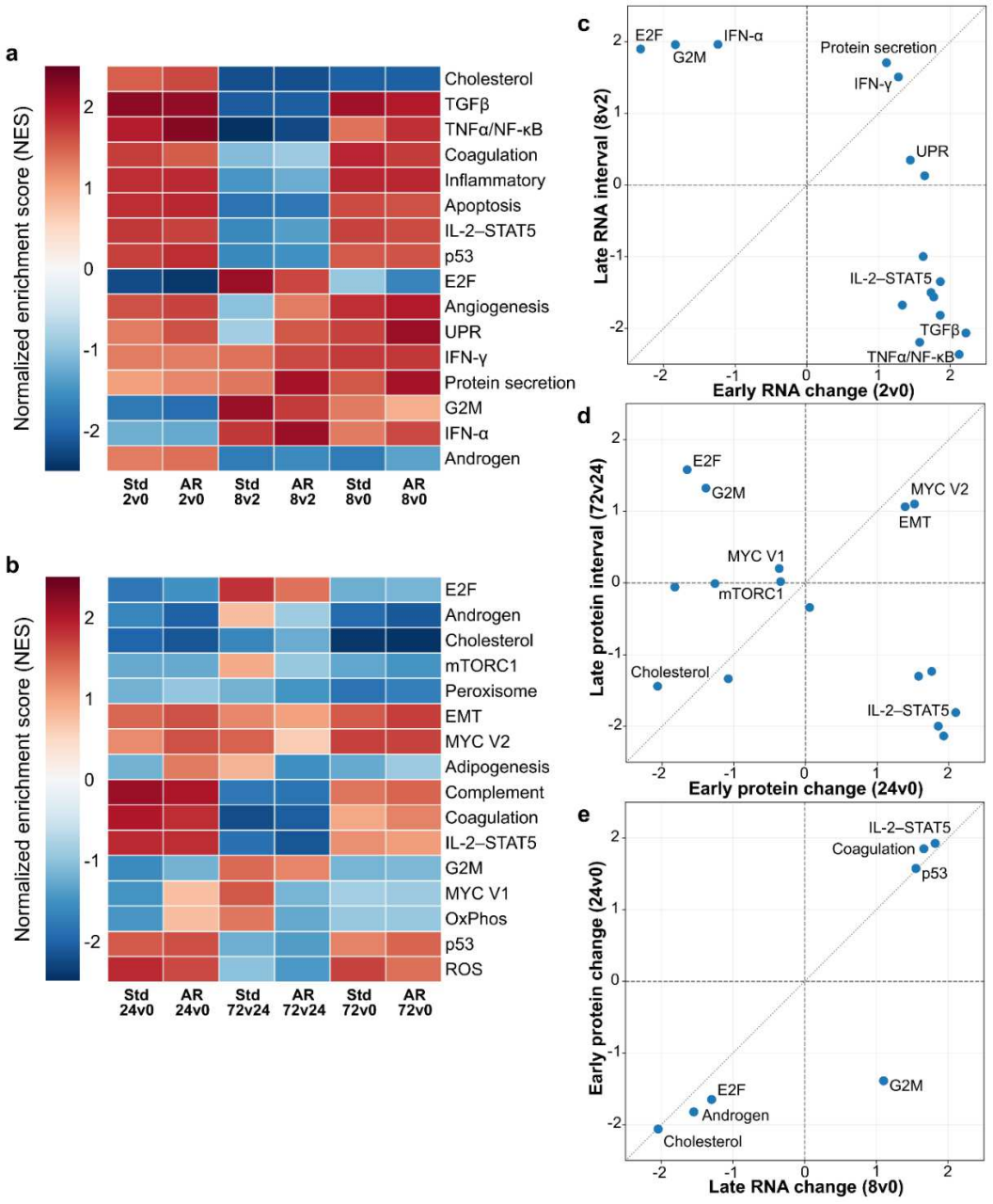


Fig. 5 | Temporal Hallmark pathway enrichment across transcriptomic and proteomic datasets. a, Transcriptomic NES for 2 h versus 0 h, 8 h versus 2 h, and 8 h versus 0 h in STD and AR cells. b, Proteomic NES for 24 h versus 0 h, 72 h versus 24 h, and 72 h versus 0 h. Positive NES indicates enrichment at the later time point. Displayed pathways were selected from significant results (RNA adjusted $p < 0.01$; protein adjusted $p < 0.05$) based on absolute NES and temporal variability. c, Mean STD/AR NES for the early versus later transcriptomic intervals. d, Corresponding proteomic comparison. e, Descriptive comparison of 8-h transcriptomic and 24-h proteomic enrichment for the seven Hallmark pathways represented in both displayed pathway sets.

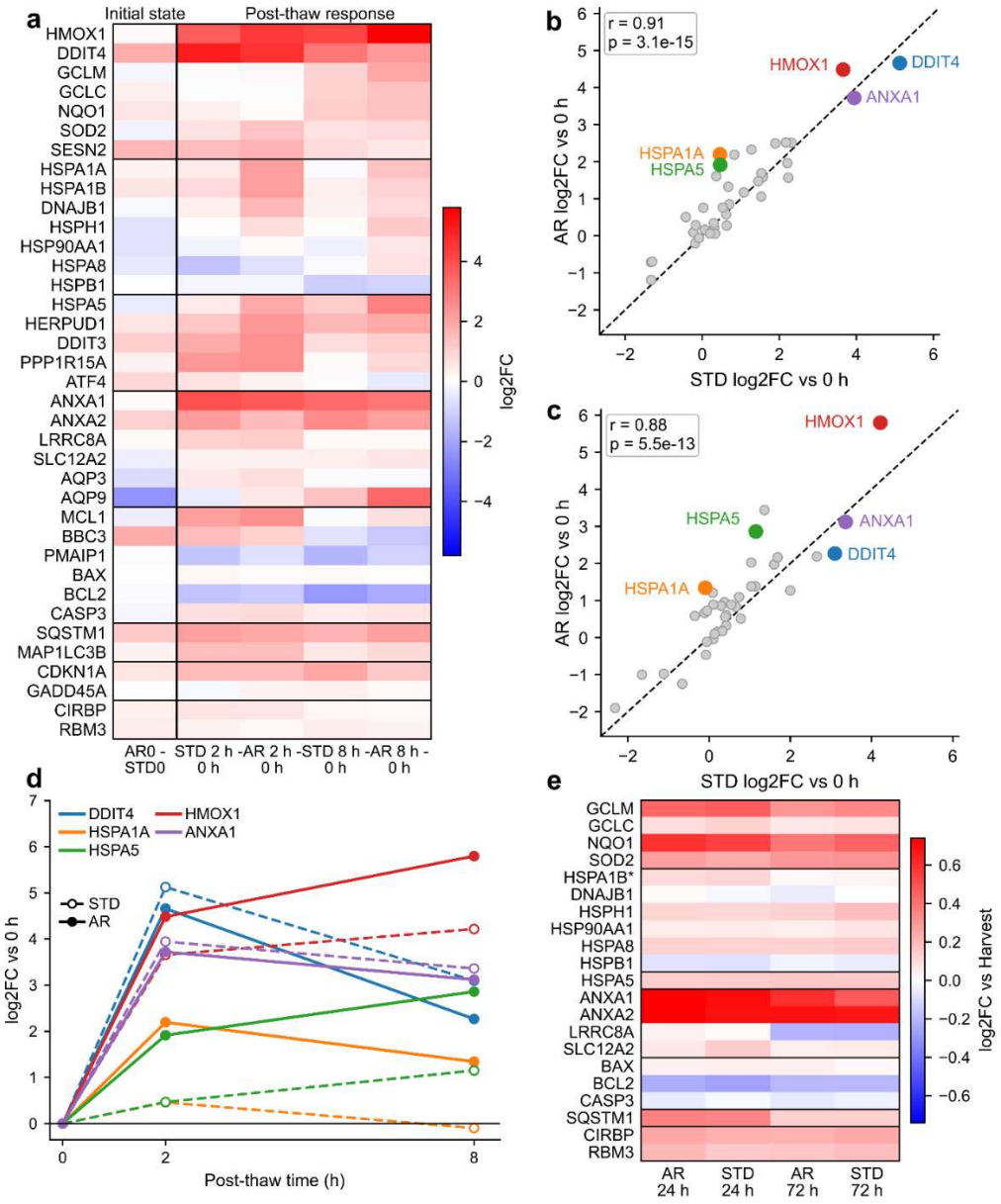


Fig. 6 | Cryostress-marker responses across transcriptomic and proteomic datasets. a, Transcriptomic log2 fold changes for 37 predefined cryostress markers. The first column compares AR with STD at 0 h; subsequent columns show 2- and 8-h changes relative to the corresponding 0-h state within each format. b,c, Concordance of STD and AR responses across the 37 markers at 2 and 8 h, respectively; Pearson *r* and two-sided *p* values are shown. d, Representative within-format marker trajectories for DDIT4, HSPA1A, HSPA5, HMOX1, and ANXA1. e, Protein-abundance changes for the 21 detected markers at 24 and 72 h relative to the shared harvest. HSPA1A was not detected in the proteomic dataset; HSPA1B* is shown as the detected inducible HSP70-family correlate. RNA-seq: *n* = 3 biological replicates per group except AR 2 h, *n* = 5; proteomics: *n* = 3 per group.

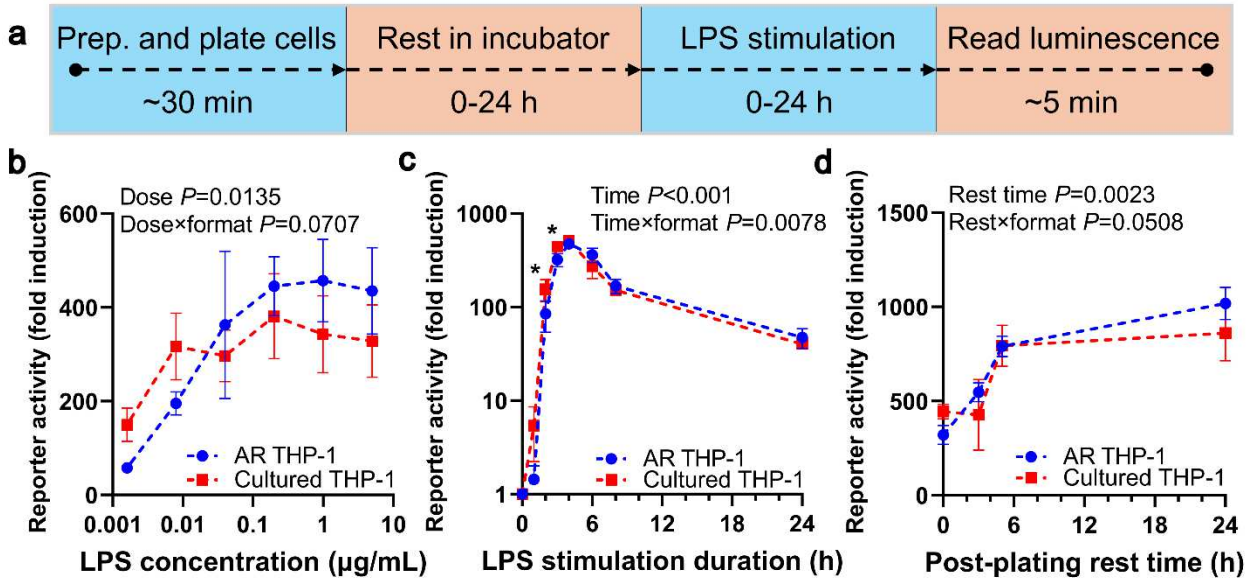


Fig. 7 | NF-κB reporter responses depend on LPS stimulation and post-plating timing. a, Experimental workflow comparing assay-ready (AR) and non-frozen cultured THP-1 NF-κB reporter cells. b, LPS concentration response following immediate stimulation for 3 h (n = 3 independent biological experiments). c, Response to 1 µg/mL LPS across stimulation durations (n = 4 independent biological experiments). d, Response after 0–24 h post-plating rest followed by 1 µg/mL LPS for 3 h (n = 4 independent biological experiments). Reporter activity is fold induction relative to the corresponding unstimulated control; points show mean ± SD. Technical triplicates in c,d were averaged within each biological experiment. Two-factor repeated-measures ANOVA with Greenhouse–Geisser correction: b, concentration $F(1.19, 2.39) = 43.96$, $p = 0.0135$; concentration × format $F(1.68, 3.35) = 6.55$, $p = 0.0707$. c, duration $F(1.19, 3.56) = 234.64$, $p < 0.001$; duration × format $F(1.43, 4.28) = 20.12$, $p = 0.0078$. d, rest time $F(1.33, 3.98) = 44.49$, $p = 0.0023$; rest time × format $F(1.86, 5.58) = 5.41$, $p = 0.0508$. *$p < 0.05$ for Holm-adjusted paired comparisons between formats; exact adjusted $p = 0.0113$ at 2 h and $p = 0.0404$ at 3 h in c.

Supplementary Files

This is a list of supplementary files associated with this preprint. Click to download.

- SupplementaryInformationScientificReports.pdf